Journal of Applied Fluid Mechanics, Vol. 18, No. 2, pp. 438-449, 2025.
Available online at www.jafmonline.net, ISSN 1735-3572, EISSN 1735-3645.
https://doi.org/10.47176/jafm.18.2.2830

Impact of Surface Roughness on the Aerodynamic Efficiency of Wind Turbines: A New CFD-based Correlation

A. Bouhelal[1†], M. N. Hamlaoui[1,2] and A. Smaili[1]

[1] *Laboratory of Green and Mechanical Development (LGMD), Ecole Nationale Polytechnique -ENP-, P.B. 182 El-Harrach, Algiers, 16200, Algeria*
[2] *Department of Civil Engineering, University of Ferhat Abbas-Setif 1, Bejaia Road, Setif, Algeria*

†*Corresponding Author Email: abdelhamid.bouhelal@g.enp.edu.dz*

ABSTRACT

The aerodynamic performance of wind turbines is significantly influenced by the design of their blades, which are engineered with advanced aerodynamic airfoils. However, the effectiveness of these designs is compromised by environmental factors such as dust, corrosion, sand, and insects, leading to alterations in blade shape and surface integrity over the turbine's operational period. These changes reduce the aerodynamic efficiency of the turbines. To assess these detrimental effects, this study utilizes a 3D Computational Fluid Dynamics (CFD) model based on the exact blade geometry. A modified version of the universal logarithmic wall function was implemented to quantify the influence of surface roughness. Comparative analyses between clean and rough blade surfaces under varying wind conditions showed that surface degradation significantly impacts the efficiency of wind turbines. Specifically, the findings indicate that surface roughness can lead to a substantial decrease in power output, with losses potentially reaching up to 35% under tested conditions. Notably, this roughness effect exhibits a critical value of $k_S^* = 1$, beyond which the impact of roughness becomes negligible. Based on these results, an exponential correlation has been proposed. This study suggests that maintaining smooth blade surfaces or minimizing roughness is crucial for optimal turbine performance, especially under high wind conditions.

Article History

Received May 4, 2024
Revised August 22, 2024
Accepted September 15, 2024
Available online December 4, 2024

Keywords:

Wind Turbine Aerodynamics
Surface Roughness Effects
Logarithmic wall function
Computational Fluid Dynamics (CFD)
Horizontal Axis Wind Turbine (HAWT)
CFD Correlation

1. INTRODUCTION

Wind turbines are deployed across diverse environmental conditions—from the cold Arctic regions to hot, sandy deserts—each presenting unique challenge. These environments often contain various contaminants like dust, dirt, ice, and insects, which accumulate on the surfaces of turbine blades. Such accumulations disrupt the smoothness of the blade surfaces, which is crucial for maintaining optimal aerodynamic performance, thus creating imperfections that affect the airflow around the blades (Manwell et al., 2010; Anderson, 2020).

These disruptions on the blade surfaces lead to diminished energy production from the affected wind turbines, deviating from their anticipated energy output. This reduction in energy yield, apart from being an engineering challenge, also presents significant economic concerns. Hence, understanding the intricate dynamics of environmental factors and their impact on wind turbine efficiency is essential for advancing both the technological and economic aspects of wind energy systems (Yigit, 2020).

Numerous studies have been conducted to explore the impact of surface roughness on the aerodynamics of wind turbine blades, utilizing both experimental and computational approaches. One notable study by Khalfellah and Koliub (2007) examined the effects of dust accumulation on the blades of Nordtank wind turbines at a dusty site in Hurghada. The research showed a definitive link between increased roughness due to dust deposition and decreased power output from the turbines. Notably, at higher wind speeds, the power reduction could exceed 50%, underlining the profound influence of dust-induced roughness on the efficiency of wind turbine operations.

In another detailed experimental study, Ramsay et al. (1995) investigated the 2D S809 airfoil under conditions that included steady-state flow and pitch oscillations. The study aimed to assess the performance losses attributable to surface roughness, using a specific grit pattern known as LEGR to simulate leading edge contamination. Results

NOMENCLATURE

CFD	Computational Fluid Dynamics	r_e	refinement factor of the GCI method
C_p	pressure coefficient	TI	turbulence intensity
F_N	normal force	U_∞	freestream wind speed
F_T	tangential force	u_τ	wall friction velocity
GCI	Grid Convergence Index	y^+	dimensionless wall distance
HAWT	Horizontal Axis Wind Turbines	y_0	aerodynamic roughness height
k	turbulence kinetic energy	ΔB	roughness function
k_S	equivalent sand grain roughness height	μ	dynamic viscosity
k_S^+	dimensionless sand grain roughness height	μ_t	turbulent viscosity
k_S^*	Normalized equivalent sand grain roughness height	ν	kinematic viscosity
MEXICO	Model Experiments in Controlled Conditions	ξ	apparent order of accuracy of the GCI method
R	blade radius	τ_w	wall shear stress
RANS	Reynolds Averaged Navier-Stokes	ρ	air density
RNG	renormalization group	ε	dissipation rate of turbulent energy
r	local blade radius	Ω	rotational wind speed

indicated a marked degradation in airfoil performance due to roughness, with significant reductions in lift and increases in drag compared to a clean, smooth airfoil. These findings underscore the critical role of surface conditions, such as leading-edge contamination, in shaping the aerodynamic performance of airfoils and consequently, the overall performance of wind turbine blades.

Further, Chakroun et al. (2004) carried out a rigorous experimental study to determine how variations in the position and size of roughness affect the aerodynamic characteristics of symmetric airfoils, specifically focusing on the NACA 0012 airfoil. The study subjected the airfoil to different roughness patterns and found that drag increased with the size of the roughness elements. This research also highlighted the significant effects of roughness at the leading edge, pointing out its substantial impact on the airfoil's aerodynamic properties.

To investigate numerically the impacts of roughness on airfoils, various numerical methods have been utilized. A study by Van Rooij and Timmer (2003) extensively examined airfoils with thicknesses between 25% and 30% using the RFOIL code, an adaptation of the XFOIL code (Drela, 1989). This research also incorporated the Snel-Houwink model (Snel el al., 1993) to account for blade rotation effects. The findings highlighted that airfoils in the 25% thickness category exhibited less sensitivity to roughness, suggesting they maintain better performance despite surface imperfections. Additionally, the study demonstrated significant rotational effects on airfoil characteristics, emphasizing the importance of considering 3D factors for a comprehensive evaluation of airfoil performance beyond traditional 2D approaches.

Ren and Ou (2009) performed numerical simulations on the NACA 63-430 airfoil, assessing the impact of different roughness sizes using the *k-ω SST* turbulence model (Menter, 2004) to solve the Reynolds-Averaged Navier-Stokes (RANS) equations. The research showed that aerodynamic coefficients rapidly changed as roughness reached a critical level, resulting in a decrease in lift and an increase in drag. Beyond this critical threshold, the changes in forces became less pronounced.

In a comparative 2D numerical analysis, Munduate and Ferrer (2009) explored the flow dynamics around the S809 airfoil using both XFOIL and Fluent. The comparison with experimental data indicated that CFD tools like Fluent can provide both qualitative and quantitative insights into the effects of surface roughness. However, XFOIL was noted to be less effective at predicting the impact of roughness, highlighting the limitations of certain numerical techniques in handling complex surface conditions on airfoils.

A review of the existing literature reveals a predominant focus on 2D studies, overlooking the impact of 3D rotation blade effects. Thus, there is a critical need to delve into these aspects. This study aims to investigate the influence of blade roughness on the aerodynamic performance of Horizontal Axis Wind Turbines (HAWTs). In order to account for roughness effects, adjustments were made to the universal standard wall law function. Utilizing Computational Fluid Dynamics (CFD) techniques, specifically the resolution of the Reynolds-Averaged Navier-Stokes (RANS) equations coupled with the high Reynolds *k-ε RNG* turbulence model, simulations were conducted for the 3D flow around the MEXICO (Model Experiments in Controlled Conditions) wind turbine across three distinct flow conditions, including attached and separated flows. ANSYS Fluent software (version 17.2) was employed for these simulations. A comparative analysis between smooth and rough blade conditions across varying wind speeds was carried out to discern the impact of roughness on rotor aerodynamic performance.

2. WIND TURBINE MODEL

This research focuses on the simulation of the MEXICO (Model Experiments in Controlled Conditions) (Snel et al., 2007) wind turbine conducted at the German Dutch Wind Tunnels (DNW). The setup involved

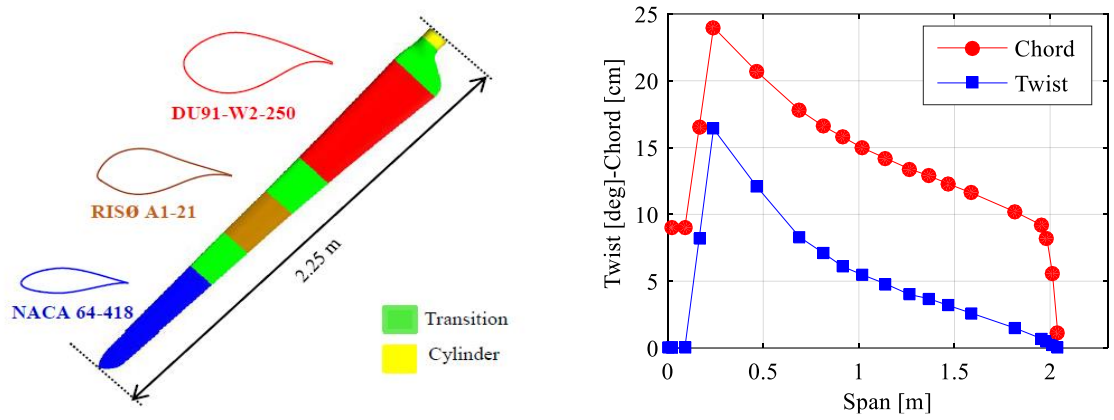

(a) (b)

Fig. 1 (a) MEXICO wind turbine blade configuration, (b) Twist and chord distributions along the MEXICO blade span (Bouhelal et al. 2022a)

A detailed examination of a three-bladed rotor with a diameter of 4.5 meters, tested within an open section measuring 9.5 x 9.5 meters squared. Each blade, measuring 2.04 meters in length, was outfitted with a sophisticated arrangement of airfoils: DU91-W2-250 at the root, RISØ A1-21 at mid-span, and NACA64-418 towards the tip (see Fig. 1). The blades incorporated 148 Kulite® pressure sensors for precise aerodynamic pressure measurement across their surfaces (Boorsma & Schepers, 2016). Force and moment data were accurately captured using a six-component balance system located at the base of the tower, converting these measurements to the rotor's center based on the model coordinate system. The experiments encompassed a range of conditions, including wind speeds from 5.5 m/s to 30 m/s, pitch angles from -5.3 to 90 degrees, and rotational speeds up to 424 rpm (Sørensen el al., 2016). The present study focuses on the no yawed test, with three wind speeds of $U_\infty = 10, 15,$ and $24\ m/s$ considered for evaluating the effect of roughness on aerodynamic performance.

3. MATHEMATICAL MODEL

3.1 Governing Equations

The fundamental equations governing the flow field are the continuity and conservation of momentum equations, commonly referred to as the Navier-Stokes equations. In this study, the flow is assumed to be steady-state, incompressible and turbulent, hence the Navier-Stokes equations are given by (Pope, 2001; Bouhelal & Smaili, 2022b):

$$\nabla . \vec{u} = 0 \tag{1}$$

$$\rho\{\nabla . (\vec{u}\vec{u}) + [\vec{\omega} \times \vec{u}]\} = -\nabla p + \nabla . \left(\bar{\bar{\tau}}\right) \tag{2}$$

Where ρ represents the density of the air, $\vec{u}$ is the vector of the velocity, and p is the static pressure. The term $\rho[\vec{\omega} \times \vec{u}]$ includes the Coriolis and centripetal accelerations due to the rotor's rotation speed. $\bar{\bar{\tau}}$ is the shear stress tensor, it can be defined by the following expression:

$$\bar{\bar{\tau}} = (\mu + \mu_t).(\nabla\vec{u} + \nabla\vec{u}^T) - \rho\frac{2}{3}k\delta_{ij} \tag{3}$$

μ and μ_t are respectively the molecular dynamic and the turbulent viscosities, k represents the turbulent kinetic energy, and δ_{ij} is the Kronecker delta.

3.2 Turbulence Modeling

For the turbulence modeling, the high Reynolds *k-ε RNG* turbulent model (Yakhot & Orszag,1986) was chosen for this study, building upon the framework of the standard *k-ε* model but with notable enhancements to handle complex flow dynamics. The *k-ε RNG* model is distinguished by its use of the Renormalization Group (RNG) theory to refine the turbulence kinetic energy dissipation rate (*ε*), enhancing its predictive accuracy in high-strain rate scenarios. This aspect makes it particularly effective for applications like wind turbines, where the flow conditions can be extremely variable and challenging to model. The proven success of this model in previous studies by Bouhelal et al., (2017, 2018a, b) further validates its capability to capture the intricate influences of turbulence, ensuring more reliable and efficient design and analysis of turbine blades from a mathematical and engineering perspective.

3.3 Rotor Rotation Modeling

To effectively incorporate the rotational movement of the turbine blades, a steady-state approximation known as the Multiple/Moving Reference Frame (MRF) technique was employed. The MRF method facilitates the transformation of the fluid motion equations into the moving frame of reference, thus enabling the derivation of steady-state solutions that accurately reflect the rotational behavior of the blades. From a mathematical standpoint, the MRF technique involves modifying the Navier-Stokes equations by adding source terms that account for the rotational effects and centrifugal forces inherent in the rotating reference frame. Numerically, this approach decouples the rotational motion from the translational motion, simplifying the computational grid and reducing the need for recalculating the entire mesh with each time step, which is a requirement in methods like the sliding mesh technique. As a result, the MRF approach offers the advantage of significantly reduced computational times (Bouhelal et al., 2018a; Hamlaoui et al., 2024).

3.4 Roughness Modeling

To model the influence of surface roughness within the CFD framework, a modification of the universally recognized standard wall function, originally formulated by Launder and Spalding (1983), was incorporated. This adapted wall function is described by the equation:

$$\frac{U_P u_\tau}{\tau_w/\rho} = \frac{1}{\kappa} ln\left(E\frac{u_\tau y_P}{\nu}\right) - \Delta B \tag{4}$$

Here, U_P and y_P denote the velocity and the distance from the blade surface to the midpoint of the neighboring cell, respectively. The variable ν represents the kinematic viscosity ($\nu = \mu/\rho$), and E is the smooth surfaces constant, set at 9.793. The term τ_w indicates the blade surface shear stress, and u_τ, the friction velocity, is given by:

$$u_\tau = {C_\mu}^{1/4} {k_P}^{1/2} \tag{5}$$

In this context, k_P refers to the turbulent kinetic energy at the cell's midpoint near the wall, and C_μ is a constant valued at 0.09.

The refinement of the wall function, as stated in Eq. (4), is underpinned by experimental observations by Nikuradse (1933) on the effects of sand grain roughness on pipe flow dynamics. Nikuradse noted that the velocity profile adjacent to rough surfaces adheres to a logarithmic distribution, identical in gradient ($1/\kappa$) but differing in intercept (ΔB). As documented in his studies. The roughness function is explicitly related to the dimensionless roughness height k_s^+, defined as:

$$k_S^+ = \frac{u_\tau k_S}{\nu} \tag{6}$$

Where k_S is roughness size of equivalent sand grain. This roughness parameter divides flow conditions into three distinct regimes: smooth ($k_S^+ < 2.25$), intermediate ($2.25 \leq k_S^+ < 90$), and rough ($k_S^+ \geq 90$). The calculations for ΔB in each regime derive from Nikuradse's findings and are further elaborated by Cebeci and Bradshaw (1977).

For the fully rough condition, the adjustment ΔB is calculated as:

$$\Delta B = \frac{1}{\kappa} ln\left(1 - C_s\, {k_S}^+\right) \tag{7}$$

Cebeci and Bradshaw (1977) also established a correlation between the aerodynamic roughness lengths (y_0) and the roughness size of equivalent sand grain (k_S), proposing:

$$k_S = \frac{E}{C_s} y_0 \tag{8}$$

For the specified default value of $C_s = 0.5$, Eq. (8) can be simplified to express the relationship between the roughness size of equivalent sand grain k_S and the aerodynamic roughness length y_0 more directly. The revised equation becomes:

$$k_S \approx 20 y_0 \tag{9}$$

The last expression indicates that $1\,mm$ of aerodynamic roughness length on a blade surface corresponds to a $20\,mm$ roughness size of an equivalent sand grain (k_S). The impact of roughness can be analyzed based on either y_0 or k_S. In this work, the analysis will primarily utilize k_S to present the results in a more general manner.

In this study, Eqs. (4) to (9) were implemented as a boundary condition at the blade surface wall to investigate the impact of surface roughness on the aerodynamic performance of the MEXICO wind turbine.

4. NUMERICAL METHOD

4.1 Computational Domain

In scenarios where the wind turbine is aligned with the wind (upwind configuration), the effects of the tower and nacelle on the rotor's aerodynamic performance are minimal and can be disregarded (Bouhelal et al. 2022a). To enhance the efficiency of the simulation and minimize computational demands, the grid was designed to explicitly represent only one of the three blades. This approach leverages the symmetry of the rotor's 120° division, using periodic boundary conditions to model the presence of the other two blades without directly simulating them. This method effectively captures the full dynamics of the rotor while optimizing the computational resources.

The 3D CAO model of the MEXICO wind turbine blade was constructed using SolidWorks, starting with the coordinates of the 2D airfoils and detailed geometric specifications presented in Fig. 1(b). The full field of computational domain was divided into two distinct areas (referenced in Fig. 2). The first area begins five blade radii upstream and extends to ten blade radii downstream for the exit boundary. This region having a radius of five blade radii. The second region is configured as a cylindrical volume with a diameter of two blade radii and a length equivalent to one blade radius. This cylindrical domain employs a moving reference frame that rotates at the wind turbine's operational speed of $\Omega = 425.1$ revolutions per minute (rpm) (see Bouhelal et al. 2018a).

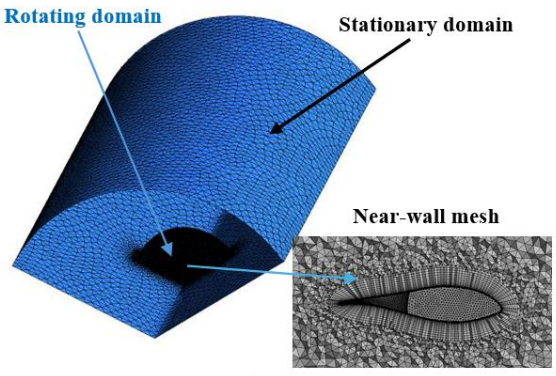

Fig. 2 Computational domain and mesh of the studied problem

4.2 Mesh Independence Study

In CFD studies, conducting a grid sensitivity test is crucial for determining the mesh independence of the results, thereby ensuring that numerical errors are reduced to a negligible level. The integrity and accuracy of a numerical simulation are often gauged by assessing the discretization error.

One widely adopted method for quantifying truncation errors is the Grid Convergence Index (GCI) (Roache, 1994), founded on the generalized extrapolation theory proposed by Richardson and Gaunt (1927). This method does not require an analytical solution to the problem but estimates the mesh-induced error using a power function related to the characteristic mesh size. The technique, in its application, has been subject to various adaptations, with the approach by Celik et al. (2008) being employed in this study.

To effectively utilize the GCI method for evaluating numerical errors, three different mesh configurations were created. These meshes progressively increased in refinement, adhering to a grid refinement factor greater than 1.3, a value chosen based on empirical evidence rather than formal theoretical derivation (Celik et al., 2008). The procedure for applying the GCI method involved the following steps:

1- The characteristic mesh size, h, is defined by:

$$h = \left[\frac{1}{N}\sum_{i=1}^{N} \Delta V_i\right]^{1/3} \tag{10}$$

where ΔV_i is the *i-th* cell's volume and N represents the number of cells in the volume.

2- Simulations are performed across these meshes to determine the values of critical variables φ, such as torque, at different levels of grid refinement:

$$r_e = \left[\frac{h_{coarse}}{h_{fine}}\right] > 1.3 \tag{11}$$

3- The apparent order of accuracy, ξ, is calculated using the formula:

$$\xi = \frac{1}{\ln(r_{e_{21}})}\left|ln\left|\frac{\varepsilon_{32}}{\varepsilon_{21}}\right| + ln\left[\frac{r_{e_{21}}^{\xi} - s}{r_{e_{32}}^{\xi} - s}\right]\right| \tag{12}$$

where: $s = sign(\varepsilon_{32}/\varepsilon_{21})$; $r_{e_{21}} = h_2/h_1$; $\varepsilon_{21} = \varphi_2 - \varphi_1$ and $\varepsilon_{32} = \varphi_3 - \varphi_2$

4- Grid Convergence Index (GCI) for the finest mesh (mesh 1 to mesh 2) is calculated as follows:

$$GCI_{fine}^{21} = \frac{1.25e_a^{21}}{r_{e_{21}}^{\xi} - 1} \tag{13}$$

where $e_a^{21} = |(\varphi_1 - \varphi_2)/\varphi_1|$, represents the relative error between mesh 1 and mesh 2.

The GCI value serves as a crucial indicator of the proximity of the computational results to the asymptotic solution. In this analysis, Eq. (12) was numerically solved for ξ using the Newton iteration method, which ensures accurate convergence to the desired precision of the results. This method is particularly effective in handling the nonlinear nature of the equation, providing a robust solution to the apparent order of accuracy calculation within the grid convergence study.

Table 1 presents the outcomes from CFD simulations investigating the airflow around a smooth blade (i.e., $\Delta B = 0$) at a wind speed of $U_\infty = 15\ m/s$ for three distinct mesh resolutions. The results show a numerical error between the coarse and medium meshes (GCI_{32}) of approximately 2%, and between the fine and medium meshes (GCI_{21}) of about 1%. This trend demonstrates that finer meshes generally lead to reduced discretization errors, though at the cost of increased computational time. Given the observed errors, the values for GCI_{32} and e_a^{21} are deemed acceptable within the context of this study, leading to the selection of the mesh configuration from case 2 for further investigative tests. This chosen mesh comprises approximately 2.7 million tetrahedral nodes within one-third of the computational domain (Fig. 2). Additionally, the mesh's first layer height is approximately $4 \times 10^{-4}\ m$, ensuring y^+ values situated in the logarithmic region ($30 < y^+ \leq 300$) on the blade surface, which is suitable for accurately capturing the boundary layer effects using high Reynolds turbulence models (i.e., with wall law function).

5. Results and Discussion

5.1 Validation of the CFD Model

In this research, the accuracy of the CFD model was evaluated by simulating three specific upwind axial wind speeds—$U_\infty = 10\ m/s$, $15\ m/s$, and $24\ m/s$—which correspond to the attached, transitional, and separated flow states, respectively, on the clean blade surface of the MEXICO rotor. The validity of the model was examined through the computation and plotting of pressure coefficients (C_p) along the mid and tip spanwise sections of the blade (at 60% and 92% span) as illustrated in Fig. 3. The results demonstrated a good agreement with experimental data across all simulated wind speeds. The pressure coefficient was normalized using the formula: $0.5\rho[(\Omega . r)^2 + U_\infty^2)]$, based on pressures calculated from the Navier-Stokes equations.

Further analysis included the calculation of axial and tangential forces along the blade (F_N and F_T), derived from

Table 1 Mesh independence study using the Grid Convergence Index (GCI)

Mesh case	Number of Nodes	Error e_a (%)	Refinement factor, r_e	GCI (%)
1	6,836,854	-	-	-
2	2,697,226	0.9928	1.3635	1.2535
3	1,171,613	1.7129	1.3204	2.1785

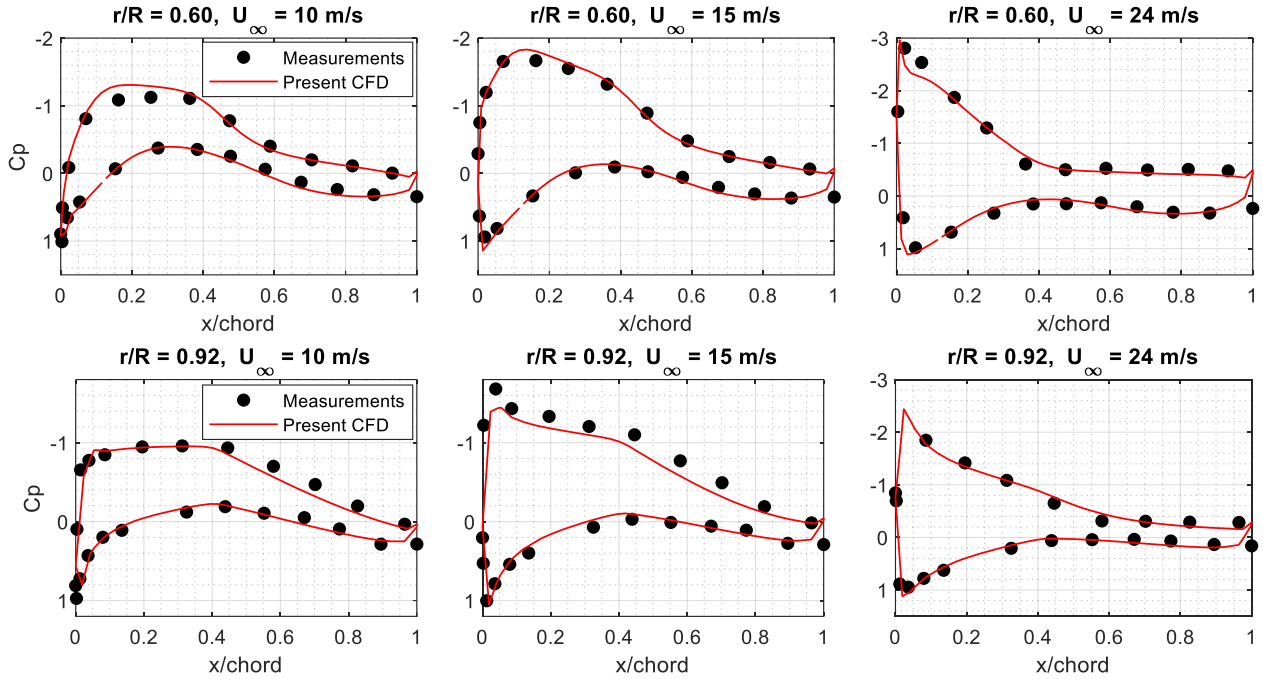

Fig. 3 Pressure coefficient distributions at the mid-spanwise (60%) and tip-spanwise (92%) sections of the blade, comparison between present CFD results and new MEXICO measurements

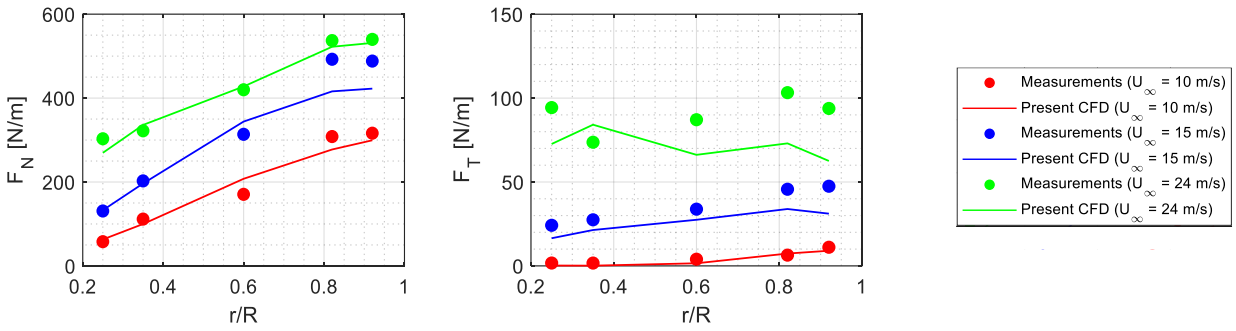

Fig. 4 Normal and tangential force distributions along the normalized blade length for the three studied wind speeds, comparison between present CFD results and new MEXICO measurements

the sectional pressure distributions, and compared with experimental findings in Fig. 4. The forces were exclusively obtained by integrating the pressure data without incorporating shear stress, as it was absent from the experimental setup. This integration employed the trapezoidal method to ensure precision in translating the pressure distributions into quantifiable force data, reinforcing the CFD model's credibility through these comprehensive comparisons. Fig. 4 shows that the forces computed align closely with the experimental data, particularly at lower and moderate wind speeds. However, a minor discrepancy is observed at higher wind speeds, where the flow predominantly exhibits separation. This divergence highlights a common challenge faced by all RANS models in accurately resolving fully separated flow conditions (Bouhelal et al., 2016, 2018b; Hamlaoui et al. 2024).

5.2 Case Study

This section discusses a numerical analysis investigating how different levels of surface roughness affect airflow around the MEXICO blade. The analysis builds on experimental findings by Khalfallah and Koliub (2007), who observed variations in aerodynamic roughness size from 0.01 mm to 0.7 mm, accumulating over periods ranging from one week to nine months in dusty environments. For this study, aerodynamic roughness heights were considered within the range of 0.01 mm to 0.1 mm, as impacts beyond this range were deemed minimal (Bouhelal et al., 2016). Additionally, the study explored the influence of a very smaller roughness value of 0.0005 mm. In addition, the results will be analyzed based on the normalized equivalent sand grain roughness height, denoted as k_S^*, where the normalization factor is 1 mm (i.e., $k_S^* = k_S(mm)/1mm$). The selected roughness values and their corresponding roughness size of an equivalent sand grain (k_S) and normalized equivalent sand grain roughness (k_S^*) values are listed in Table 2.

5.3 Impact of Surface Roughness on Aerodynamic Forces

Figure 5 illustrates the impact of various normalized equivalent sand grain roughness heights on the normal (F_N) and tangential (F_T) force distributions along the

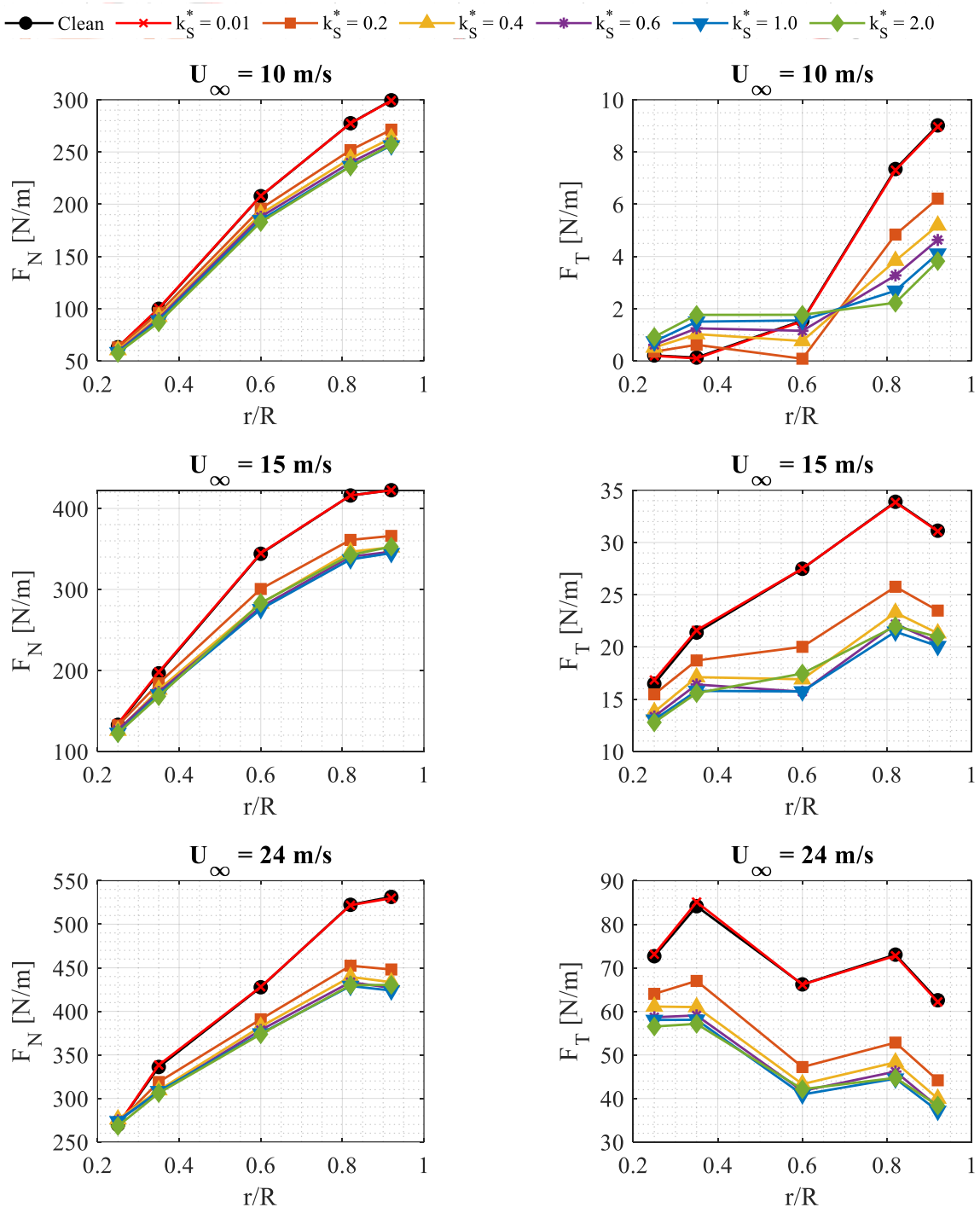

Fig. 5 Normal (F_N) and tangential (F_T) force distributions along the normalized blade length, comparison of different normalized equivalent sand grain roughness heights

Table 1 Values of the studied roughness heights

Aerodynamic roughness length y_0	Equivalent sand grain roughness height k_S	Normalized equivalent sand grain roughness height k_S^*
0.0005 mm	0.01 mm	0.01
0.01 mm	0.2 mm	0.2
0.02 mm	0.4 mm	0.4
0.03 mm	0.6 mm	0.6
0.05 mm	1 mm	1
0.1 mm	2 mm	2

normalized blade length of a wind turbine under different wind speeds: $U_\infty = 10\ m/s$, $15\ m/s$, and $24\ m/s$.

At the lowest wind speed of 10 m/s, the data show a consistent increase in both F_N and F_T from the hub ($r/R = 0.2$) to the tip ($r/R = 1$) across all roughness levels, indicating a largely attached flow with minimal influence from surface roughness. The closely grouped lines for different roughness values suggest that at lower wind speeds, the boundary layer remains stable and less susceptible to the effects of roughness, thereby maintaining efficient aerodynamic performance.

As the wind speed increases to $15\ m/s$, the effects of roughness become more noticeable, particularly on the tangential forces. While normal forces continue to show a general increase from hub to tip, the peak values of tangential forces shift slightly towards the hub, and the magnitude decreases notably at higher roughness levels. This indicates the onset of flow separation or stall, particularly at the outer sections of the blade where the aerodynamic loads are crucial for energy production. Higher roughness disrupts the smooth flow of air, leading to increased turbulence and earlier transition from laminar to turbulent flow, which reduces the aerodynamic efficiency.

At the highest tested wind speed of $24\ m/s$, the disruption caused by blade surface roughness is most severe. Both F_N and F_T show significant reductions at higher surface roughness values, with tangential forces decreasing dramatically across the normalized blade length. This pattern suggests massive separation of the flow, where the increased turbulence and adverse pressure gradients caused by the roughness lead to a breakdown of the boundary layer. This breakdown is especially detrimental at high wind speeds where the force distributions are crucial for maintaining high power output. The severe decrease in tangential forces across the entire blade length at this speed indicates that the turbine's ability to generate torque and thus power is substantially compromised by the rough surface.

5.4 Influence of Surface Roughness on the Pressure Coefficient

Figure 6 illustrates the pressure coefficient (C_p) distributions along the normalized chord at the blade span position $r/R = 0.6$ for the MEXICO wind turbine under varying wind speeds ($10\ m/s$, $15\ m/s$, and $24\ m/s$) and different normalized surface roughness levels.

At a wind speed of $10\ m/s$, the C_p curves display a characteristic shape with a sharp peak near the leading edge followed by a gradual decline towards the trailing edge, indicating efficient aerodynamic performance with a well-attached flow over most of the blade surface. The influence of roughness at this low wind speed is subtle, with slight deviations in C_p values particularly towards the trailing edge as roughness increases, suggesting minor disruptions in airflow due to increased airfoil surface due to the roughness.

When the wind speed increases to $15\ m/s$, the deviations in C_p curves become more pronounced with increasing roughness. The peak near the leading edge is less sharp and shifts slightly downstream, which may indicate a delay in the flow separation point. This shift suggests that roughness begins to affect the flow dynamics more significantly, causing an earlier transition from laminar to turbulent flow along the blade surface, thus altering the pressure distribution and potentially reducing lift while increasing drag. To substantiate this observation, the distribution of turbulence intensity under varying roughness heights will be analyzed in the following subsections.

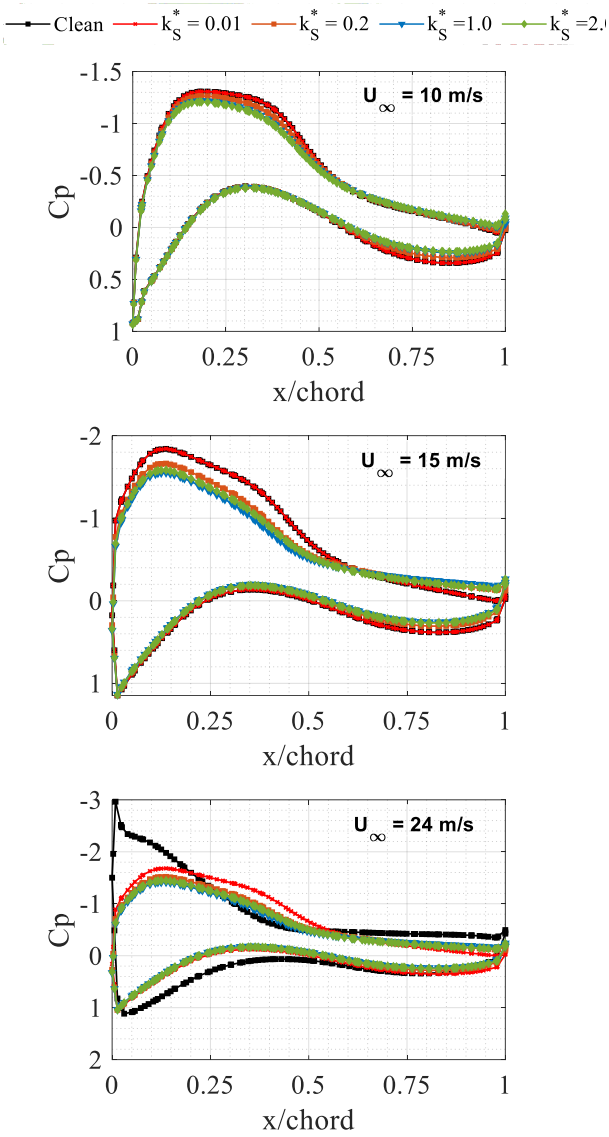

Fig. 6 Pressure coefficient (C_p) distributions along the normalized chord at the $r/R = 0.6$ blade span, comparison of different normalized equivalent sand grain roughness heights

At the highest wind speed of $24\ m/s$, the impact of roughness is most evident. The C_p curves show significant alterations across all roughness levels, with the peaks becoming more flattened and the overall distribution indicating a higher level of turbulent flow across the blade. The changes in the C_p distribution at this speed suggest a substantial influence of roughness on the blade aerodynamics, leading to a more pronounced flow separation and increased aerodynamic losses. The

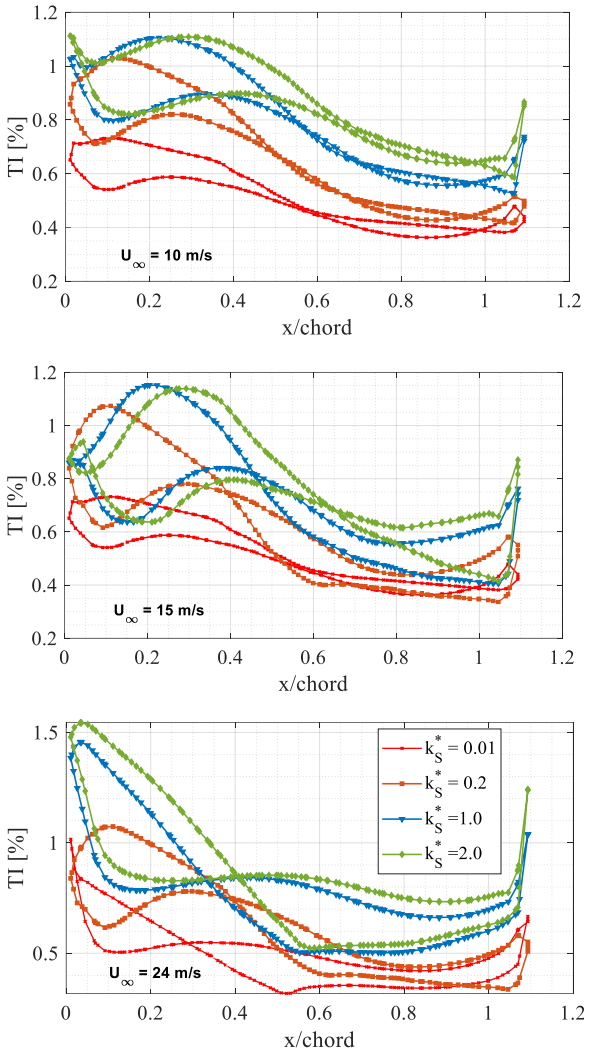

Fig. 7 Turbulence intensity (TI) distributions along the normalized chord at the $r/R = 0.6$ blade span, comparison of different normalized equivalent sand grain roughness heights

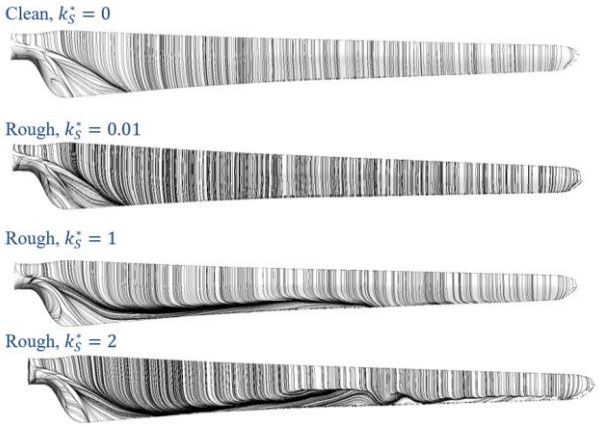

Fig. 8 Streamlines on the suction side of the blade, comparison of different normalized equivalent sand grain roughness heights

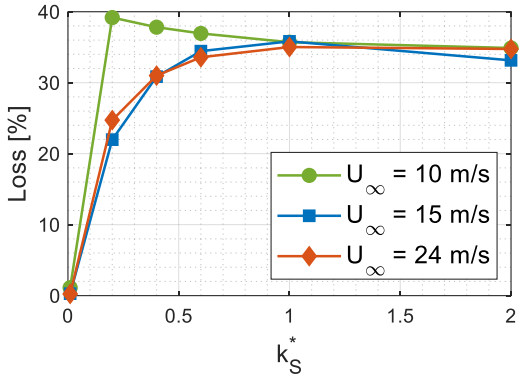

Fig. 9 Variation of power loss versus different normalized equivalent sand grain roughness heights at various wind speeds

presence of high roughness levels exacerbates these effects, resulting in a more disrupted flow and less efficient energy extraction from the wind.

5.5 Influence of Surface Roughness on the Turbulence Intensity and Flow Separation

Figs. 7 and 8 offer a detailed view of how different levels of surface roughness impact the aerodynamic behavior of wind turbine blades through visualizations of turbulence intensity (TI) and streamline patterns on the suction side of the blade.

Figure 7 presents the turbulence intensity (TI) distributions along the normalized chord at $r/R = 0.6$ for the three studied wind speeds (10 m/s, 15 m/s, 24 m/s) across a range of normalized roughness heights. At 10 m/s, the TI remains relatively low across all roughness levels, with a noticeable but low increase in turbulence as roughness increases. This suggests that at lower speeds, the blade maintains a smoother aerodynamic profile with less pronounced effects from surface imperfections. As the wind speed increases to 15 m/s and 24 m/s, the impact of roughness becomes markedly more significant. The curves show higher peaks and wider distributions of turbulence intensity, particularly for higher roughness values, indicating increased aerodynamic disturbances. At 24 m/s, the turbulence intensity is particularly high across the blade, especially for roughness values of $k_S^* = 1$ and $k_S^* = 2$, demonstrating severe disruptions in flow, tending leading to reduced aerodynamic efficiency.

Figure 8 visualizes the streamlines on the suction side of the blade for different surface roughness levels under a clean condition and three roughness conditions ($k_S^* =$ 0.01, 1 and 2) calculated for the design wind speed of 15 m/s. The streamline patterns offer a direct visual representation of flow behavior across the blade surface. In the clean condition, streamlines are smooth and closely follow the blade contour, indicating efficient and attached flow. As roughness increases to $k_S^* = 0.01$, slight disturbances begin to appear near the leading edge, suggesting the onset of flow separation. At $k_S^* = 1$ and $k_S^* = 2$, the streamlines become increasingly chaotic and detached, especially towards the trailing edge of the blade. This detachment is indicative of significant flow separation, which is a critical factor in aerodynamic

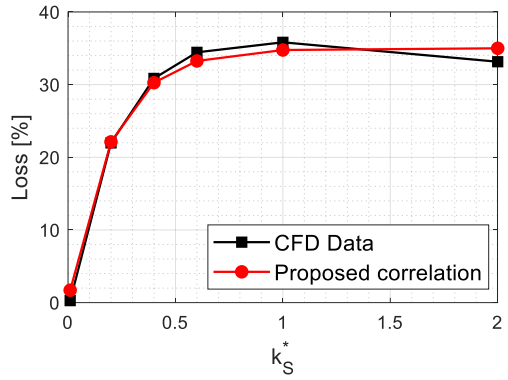

Fig. 10 Comparison of power loss variation with different normalized equivalent sand grain roughness heights, actual CFD data versus proposed correlation

performance loss, as disrupted flow cannot effectively contribute to lift and instead increases drag.

5.6 Impact of Surface Roughness on Wind Turbine Power Efficiency

Figure 9 illustrates the variation in power loss across different normalized equivalent sand grain roughness heights at various wind speeds ($10\ m/s$, $15\ m/s$, and $24\ m/s$). For the three tested wind speeds, the increase in roughness heights leads to an initial rapid rise in power loss, peaking at a roughness height of around $k_S^* = 1$. Beyond this point, the power loss stabilizes, indicating that further increases in roughness do not significantly affect the loss in power, which remains constant at about 35%. It is also observed that very fine roughness ($k_S^* = 0.01$) has a negligible impact on power efficiency for the three tested cases. The power loss for the wind speeds of $15\ m/s$ and $24\ m/s$ exhibited close similarities. However, at $10\ m/s$, there was a distinct peak of approximately 39% before reaching the critical stabilization value of $k_S^* = 1$. This figure demonstrates that while roughness significantly impacts power loss, particularly up to a critical roughness height, there seems to be a limit to its effect.

Once a certain roughness threshold is reached, additional increases do not translate into further power losses. This suggests a non-linear relationship between surface roughness and aerodynamic efficiency, where the detrimental effects of roughness are most pronounced at moderate levels of surface imperfection and stabilize beyond a specific point ($k_S^* = 1$). Moreover, higher wind speeds exacerbate the impact of roughness, but the relative increase in power loss does not continue indefinitely, stabilizing once a certain roughness level is reached. This highlights the complex interplay between surface conditions and operational environments in wind turbine performance.

5.7 Proposed Correlation between Power Loss and Roughness Height

In this study, an innovative correlation was developed to determine the power loss of a wind turbine as a function of normalized roughness heights (k_S^*). This correlation was derived by fitting the CFD data illustrated in Fig. 9. Notably, the power losses at wind speeds of $15\ m/s$ and $24\ m/s$ were observed to be similar, and since the relationship between power loss and normalized roughness height is non-linear, the following correlation has been proposed: $Loss(k_S^*) = a.exp\ (-b.k_S^*) + c$. To determine the constants a, b and c, boundary conditions were set where the loss for a clean blade is zero (i.e., Loss at $k_S^* = 0$ is zero), and the loss at infinity approaches 35%, consistent with observations from Fig. 9. A mid-point was also utilized to solve the system of equations, resulting in the following correlation for power loss:

$$Loss\ [\%] = 35 \times [-exp(-5k_S^*) + 1\ ] \qquad (14)$$

This correlation was plotted alongside actual CFD data in Fig. 10, revealing a good agreement and thereby validating its accuracy. As a result, it can be utilized to estimate power or torque losses for a given normalized roughness (k_S^*). However, it's important to note that this model is only applicable for tip speed ratios of 7 or lower, as wind speeds exceeding this threshold, such as the $10\ m/s$ case (tip speed ratio of 10), are not covered by this correlation below the critical value of $k_S^* = 1$.

6. CONCLUSION

In this study, a comprehensive numerical investigation was conducted to assess the behavior of turbulent flow around a Horizontal Axis Wind Turbine (HAWT) under various degrees of surface roughness ranging from 0.01 mm to 0.1 mm. This study spanned from scenarios of fully attached flow to significantly separated flow states. The high Reynolds *k-ε RNG* turbulence model was employed to provide closure to the Reynolds-Averaged Navier-Stokes (RANS) equations, and the influence of roughness was integrated through modifications to the logarithmic wall function. Utilizing 3D Computational Fluid Dynamics (CFD) methods, this research has highlighted several critical insights:

- Enhanced 3D CFD simulations provided a detailed look at how surface roughness influences aerodynamic forces, showcasing a reduction in both normal (F_N) and tangential (F_T) forces with increasing roughness, particularly under high wind speeds where the impact is most severe. The CFD results indicated that at a wind speed of 24 m/s, the introduction of roughness with a normalized height of $k_S^* = 1$ led to a reduction in F_N and F_T by approximately 20% and 18%, respectively.
- The study found that increased roughness significantly disrupts the pressure coefficient (C_p) distributions along the blade chord, leading to earlier flow separation and a transition to turbulent flow conditions. Specifically, at a roughness height of $k_S^* = 1$, the C_p near the leading edge showed a reduction of up to 15%, contributing to premature flow separation.
- The analysis of turbulence intensity (*TI*) and streamline behaviors under varying degrees of roughness revealed that increased surface roughness leads to heightened turbulence near the blade surface. This, in turn, affects the flow dynamics, contributing

to more chaotic and detached flow patterns, indicative of significant aerodynamic penalties. The *TI* increased by up to 30% near the blade surface at higher roughness levels $k_S^* = 1$, leading to more pronounced flow separation along the chord.

- Power loss analysis demonstrated that surface roughness up to a critical value ($k_S^* = 1$) can lead to significant efficiency reductions, with losses reaching up to 35% at higher wind speeds, particularly at 24 m/s. This impact is especially severe in separated flow regimes, where the increase in roughness exacerbates turbulence and flow separation, leading to marked performance degradation. Beyond this roughness threshold, the power loss stabilizes, indicating a diminishing return on further increases in roughness.
- The results highlighted the non-linear relationship between roughness and power loss, emphasizing the critical need to maintain blade smoothness, especially under high-speed conditions to optimize turbine efficiency. Based on the obtained CFD results, an exponential correlation between power loss and roughness height, valid for tip speed ratios of 7 or lower, has been proposed.

According to the presented results, alongside findings from previous studies, the impacts of blade surface roughness on the aerodynamics of wind turbines can be summarized as follows: Surface roughness disrupts the smooth airflow over the blades, disturbing the pressure distribution on the blade surface, which leads to increased turbulence, earlier flow separation, and reduced aerodynamic efficiency. This results in decreased lift and increased drag, collectively diminishing the overall performance of the turbine in a non-linear manner, particularly under high wind and turbulent conditions.

The comparative analysis between smooth and rough blade conditions highlights the critical importance of minimizing surface roughness to maintain turbine efficiency, particularly in high wind speed and turbulent flow environments. This study provides a solid foundation for the design and optimization of turbine blades, demonstrating the necessity for meticulous surface engineering to mitigate the detrimental effects of roughness on aerodynamic performance. These findings not only reinforce current best practices in turbine maintenance but also open avenues for future research focused on optimizing blade designs to enhance performance across a wide range of operational conditions.

ACKNOWLEDGEMENTS

The data for this study were supplied by the consortium behind the EU FP5 project MEXICO (Model rotor EXperiments In COntrolled conditions), involving nine European partners.

CONFLICT OF INTEREST

The authors declare no conflict of interest.

AUTHORS CONTRIBUTION

Abdelhamid Bouhelal: Conceptualization, Methodology, Software, Validation, Formal Analysis, Investigation, Resources, Data Curation, Writing of the Original Draft; Writing of the Final Manuscript, Review and Editing, Visualization. **Mohammed Nadjib Hamlaoui:** Methodology, Validation, Review and Editing. **Arezki Smaili:** Supervision, Methodology, Review and Editing.

REFERENCES

Anderson, C. (2020). *Wind turbines: Theory and practice*. Cambridge University Press. https://doi.org/10.1017/9781108478328

Boorsma, K., & Schepers, J. G. (2016). *Rotor experiments in controlled conditions continued: New Mexico.* Journal of Physics: Conference Series. IOP Publishing. https://doi.org/10.1088/1742-6596/753/2/022004

Bouhelal, A., & Smaili, A. (2022a). *Introduction à la CFD (Computational Fluid Dynamics).* Ecole Nationale Polytechnique. https://hal.science/hal-04427690/document

Bouhelal, A., Guerri, O., Smaili, A., & Masson, C. (2018a). *Contribution to the aerodynamic study of the air-sand flow around a wind turbine blade installed in desert environment of Algeria*. 2018 International Conference on Wind Energy and Applications in Algeria (ICWEAA) (pp. 1-6). IEEE. https://doi.org/10.1109/ICWEAA.2018.8605050

Bouhelal, A., Smaili, A., & Guerri, O. (2016). Numerical study of an horizontal axis wind turbine rotor: assessments of turbulence modeling. *10 èmes Journées de Mécanique de l'EMP (JM'10–EMP)*, 12-13.

Bouhelal, A., Smaili, A., Guerri, O., & Masson, C. (2017, December). *Comparison of BEM and full Navier-Stokes CFD methods for prediction of aerodynamics performance of HAWT rotors.* 2017 International Renewable and Sustainable Energy Conference (IRSEC). IEEE. https://doi.org/10.1109/IRSEC.2017.8477247

Bouhelal, A., Smaili, A., Guerri, O., & Masson, C. (2018b). Numerical investigation of turbulent flow around a recent horizontal axis wind Turbine using low and high Reynolds models. *Journal of Applied Fluid Mechanics, 11*(1), 151-164. https://doi.org/10.29252/jafm.11.01.28074

Bouhelal, A., Smaili, A., Guerri, O., & Masson, C. (2022b). Numerical investigations on the fluid behavior in the near wake of an experimental wind turbine model in the presence of the nacelle. *Journal of Applied Fluid Mechanics, 16*(1), 21-33. https://doi.org/10.47176/jafm.16.01.1382

Cebeci, T., & Bradshaw, P. (1977). *Momentum transfer in boundary layers.* Washington.

Celik, I. B., Ghia, U., Roache, P. J., & Freitas, C. J. (2008). Procedure for estimation and reporting of uncertainty due to discretization in CFD applications. *Journal of fluids Engineering-Transactions of the ASME, 130*(7). https://doi.org/10.1115/1.2960953

Chakroun, W., Al-Mesri, I., & Al-Fahad, S. (2004). Effect of surface roughness on the aerodynamic characteristics of a symmetrical airfoil. *Wind Engineering, 28*(5), 547-564. https://doi.org/10.1115/1.1624614

Drela, M. (1989, June). *XFOIL: An analysis and design system for low Reynolds number airfoils.* Low Reynolds Number Aerodynamics: Proceedings of the Conference Notre Dame, Indiana, USA, Berlin, Heidelberg: Springer Berlin Heidelberg. https://doi.org/10.1007/978-3-642-84010-4_1

Hamlaoui, M. N., Bouhelal, A., Smaili, A., & Fellouah, H. (2024). An engineering approach to improve performance predictions for wind turbine applications: comparison with full navier-stokes model and experimental measurements. *Journal of Applied Fluid Mechanics, 17*(7), 1379-1397. https://doi.org/10.47176/jafm.17.7.2404

Khalfallah, M. G., & Koliub, A. M. (2007). Effect of dust on the performance of wind turbines. *Desalination, 209*(1-3), 209-220. https://doi.org/10.1016/j.desal.2007.04.030

Launder, B. E., & Spalding, D. B. (1983). *The numerical computation of turbulent flows.* Numerical prediction of flow, heat transfer, turbulence and combustion. Pergamon. https://doi.org/10.1016/B978-0-08-030937-8.50016-7

Manwell, J. F., McGowan, J. G., & Rogers, A. L. (2010). *Wind energy explained: theory, design and application.* John Wiley & Sons. https://doi.org/10.1002/9781119994367

Menter, F. R. (1994). Two-equation eddy-viscosity turbulence models for engineering applications. *AIAA Journal, 32*(8), 1598-1605. https://doi.org/10.2514/3.12149

Munduate, X., & Ferrer, E. (2009, January). *CFD predictions of transition and distributed roughness over a wind turbine airfoil.* 47th AIAA aerospace sciences meeting including the new horizons forum and aerospace exposition. https://doi.org/10.2514/6.2009-269

Nikuradse, J. (1933). Stromungsgesetze in rauhen Rohren. *Vdi-Forschungsheft, 361*, 1.

Pope, S. B. (2001). Turbulent flows. *Measurement Science and Technology, 12*(11), 2020-2021. https://doi.org/10.1088/0957-0233/12/11/705

Ramsay, R. F., Hoffman, M. J., & Gregorek, G. M. (1995). *Effects of grit roughness and pitch oscillations on the S809 airfoil.* National Renewable Energy Lab. (NREL), Golden, CO (United States). https://doi.org/10.2172/205563

Ren, N., & Ou, J. (2009). *Numerical simulation of surface roughness effect on wind turbine thick airfoils*. 2009 Asia-Pacific power and energy engineering conference. IEEE. https://doi.org/10.1109/APPEEC.2009.4918540

Richardson, L. F., & Gaunt, J. A. (1927). VIII. The deferred approach to the limit. *Philosophical Transactions of the Royal Society of London. Series A, containing papers of a mathematical or physical character, 226*(636-646), 299-361. https://doi.org/10.1098/rsta.1927.0008

Roache, P. J. (1994). Perspective: A method for uniform reporting of grid refinement studies. https://doi.org/10.1115/1.2910291

Sagol, E., Reggio, M., & Ilinca, A. (2013). Issues concerning roughness on wind turbine blades. *Renewable and Sustainable Energy Reviews, 23*, 514-525. https://doi.org/10.1016/j.rser.2013.02.034

Snel, H., Houwink, R., Bosschers, J., Piers, W. J., Van Bussel, G. J., & Bruining, A. (1993). Sectional prediction of sD effects for stalled flow on rotating blades and comparison with measurements.

Snel, H., Schepers, J. G., & Montgomerie, B. (2007). *The MEXICO project (Model Experiments in Controlled Conditions): The database and first results of data processing and interpretation.* Journal of Physics: Conference Series. IOP Publishing. https://doi.org/10.1088/1742-6596/75/1/012014

Sørensen, N. N., Zahle, F., Boorsma, K., & Schepers, G. (2016, September). *CFD computations of the second round of MEXICO rotor measurements*. Journal of Physics: Conference Series. IOP Publishing. https://doi.org/10.1088/1742-6596/753/2/022054

Van Rooij, R. P. J. O. M., & Timmer, W. A. (2003). Roughness sensitivity considerations for thick rotor blade airfoils. *Journal of Solar Energy Engineering 125*(4), 468-478. https://doi.org/10.1115/1.1624614

Yakhot, V., & Orszag, S. A. (1986). Renormalization group analysis of turbulence. I. Basic theory. *Journal of Scientific Computing, 1*(1), 3-51. https://doi.org/10.1007/BF01061452

Yigit, C. (2020). Effect of air-ducted blade design on horizontal axis wind turbine performance. *Energies*, 13(14), 3618.